Active contours with selective local or global segmentation: A new formulation and level set method

Kaihua Zhang [a], Lei Zhang [a,*], Huihui Song [b], Wengang Zhou [b]

[a] Dept. of Computing, The Hong Kong Polytechnic University, Hong Kong, China
[b] Department of Electronic Engineering and Information Science, University of Science and Technology of China, Hefei 230027, People's Republic of China

A B S T R A C T

A novel region-based active contour model (ACM) is proposed in this paper. It is implemented with a special processing named *Selective Binary and Gaussian Filtering Regularized Level Set (SBGFRLS)* method, which first selectively penalizes the level set function to be binary, and then uses a Gaussian smoothing kernel to regularize it. The advantages of our method are as follows. First, a new region-based signed pressure force (SPF) function is proposed, which can efficiently stop the contours at weak or blurred edges. Second, the exterior and interior boundaries can be automatically detected with the initial contour being anywhere in the image. Third, the proposed ACM with SBGFRLS has the property of selective local or global segmentation. It can segment not only the desired object but also the other objects. Fourth, the level set function can be easily initialized with a binary function, which is more efficient to construct than the widely used signed distance function (SDF). The computational cost for traditional re-initialization can also be reduced. Finally, the proposed algorithm can be efficiently implemented by the simple finite difference scheme. Experiments on synthetic and real images demonstrate the advantages of the proposed method over geodesic active contours (GAC) and Chan–Vese (C–V) active contours in terms of both efficiency and accuracy.

© 2009 Elsevier B.V. All rights reserved.

1. Introduction

Image segmentation is a fundamental problem in image processing and computer vision. Extensive study has been made and many techniques have been proposed [1,2], among which the ACM [1,3–6] is one of the most successful methods. The basic idea of ACM is to evolve a curve under some constraints to extract the desired object. According to the nature of constraints, the existing ACMs can be categorized into two types: edge-based models [1,3,4,6,10,12,18,20] and region-based models [5,7,8,11,14–17].

One of the most popular edge-based models is the GAC model [3,4], which utilizes image gradient to construct an edge stopping function (ESF) to stop the contour evolution on the object boundaries. Usually, a positive, decreasing and regular ESF $g(|\nabla I|)$ is used such that $\lim_{t\to\infty} g(t) = 0$. For instance,

$$g(|\nabla I|) = \frac{1}{1 + |\nabla G_\sigma * I|^2}, \qquad (1)$$

where $G_\sigma * I$ denotes convolving image I with a Gaussian kernel whose standard deviation is σ. However, for digital images the discrete gradients are bounded and then the ESF in Eq. (1) will never be zero on edges. Some edge-based ACMs introduce a balloon force term to shrink or expand the contour, yet it is difficult to design the balloon force. If the balloon force is large, the contour will pass through the weak edge of the object. On the other hand, if the balloon force is not large enough, the contour may not pass through the narrow part of the object. In addition, the edge-based models are prone to local minimum, failing to detect the exterior and interior boundaries when the initial contour is far from the desired object boundary.

Region-based ACMs have many advantages over edge-based ones. First, region-based models utilize the statistical information inside and outside the contour to control the evolution, which are less sensitive to noise and have better performance for images with weak edges or without edges. Second, they are significantly less sensitive to the location of initial contour and then can efficiently detect the exterior and interior boundaries simultaneously. One of the most popular region-based models is the C–V model [5], which is based on Mumford–Shah segmentation techniques [8] and has been successfully applied to binary phase segmentation.

As pointed in [5], the C–V model can automatically detect all of the contours, no matter where the initial contour starts in the image. So we can say that the C–V model has the global segmentation property to segment all objects in an image. Comparatively, the GAC model can only extract the object when the initial contour

* Corresponding author. Tel.: +852 27667355.
E-mail addresses: zhkhua@mail.ustc.edu.cn (K. Zhang), cslzhang@comp.polyu.edu.hk (L. Zhang), freebird@mail.ustc.edu.cn (H. Song), zhwg@mail.ustc.edu.cn (W. Zhou).

surrounds its boundary, and it cannot detect the interior contour without setting the initial one inside the object. Thus we can say that the GAC model possesses local segmentation property which can only segment the desired object with a proper initial contour.

In this paper, we propose a new region-based ACM, which shares the advantages of the C–V and GAC models. We utilize the statistical information inside and outside the contour to construct a region-based signed pressure force (SPF) function [9], which is able to control the direction of evolution, to substitute the ESF. The proposed SPF function has opposite signs around the object boundary, so the contour can shrink when it is outside the object or expand when inside the object.

We propose a novel level set method, i.e. SBGFRLS, to implement our model. It improves the traditional level set methods by avoiding the calculation of SDF and re-initialization [13]. We use a selective step, which first penalizes level set function to be binary, and then uses a Gaussian filter to regularize it. The Gaussian filter can make the level set function smooth and the evolution more stable. It is worth noting that the SBGFRLS method is general and robust, and it can be applied to classical ACMs, such as GAC model [3,4], C–V model [5], PS model [14,15], and LBF model [11,24]. Furthermore, computational complexity analysis shows that the SBGFRLS method is more efficient than the traditional level set methods. In addition, the proposed model implemented with SBGFRLS has a property of selective local or global segmentation, which can not only extract the desired objects, but also accurately extract all the objects with interior and exterior boundaries.

This paper is organized as follows: In Section 2, we review the classic GAC and C–V models. Section 3 describes the formulation of our method and how to construct the region-based SPF function. The numerical method of the proposed model is also summarized in this section. Furthermore, we give detailed explanations about applying our model to segment multi-objects with different intensities. The advantages of our model over the GAC and C–V models are also discussed. Section 4 validates our method by extensive experiments on synthetic and real images. Section 5 concludes the paper.

2. The GAC and C–V models

2.1. The GAC model

Let Ω be a bounded open subset of R^2 and $I: [0, a] \times [0, b] \to R^+$ be a given image. Let $C(q): [0, 1] \to R^2$ be a parameterized planar curve in Ω. The GAC model is formulated by minimizing the following energy functional:

$$E^{\text{GAC}}(C) = \int_0^1 g(|\nabla I(C(q))|)|C'(q)|dq, \tag{2}$$

where g is the ESF as in Eq. (1).

Using calculation of variation [19], we could get the Euler–Lagrange equation of Eq. (2) as follows:

$$C_t = g(|\nabla I|)\kappa\vec{N} - \left(\nabla g \cdot \vec{N}\right)\vec{N}, \tag{3}$$

where κ is the curvature of the contour and $\vec{N}$ is the inward normal to the curve. Usually a constant velocity term α is added to increase the propagation speed. Then Eq. (3) can be rewritten as

$$C_t = g(|\nabla I|)(\kappa + \alpha)\vec{N} - \left(\nabla g \cdot \vec{N}\right)\vec{N}. \tag{4}$$

The corresponding level set formulation is as follows:

$$\frac{\partial \phi}{\partial t} = g|\nabla \phi|\left(\text{div}\left(\frac{\nabla \phi}{|\nabla \phi|}\right) + \alpha\right) + \nabla g \cdot \nabla \phi, \tag{5}$$

where α is the balloon force, which controls the contour shrinking or expanding.

2.2. The C–V model

Chan and Vese [5] proposed an ACM which can be seen as a special case of the Munford–Shah problem [8]. For a given image I in domain Ω, the C–V model is formulated by minimizing the following energy functional:

$$E^{\text{CV}} = \lambda_1 \int_{\text{inside}(C)} |I(x) - c_1|^2 dx + \lambda_2 \int_{\text{outside}(C)} |I(x) - c_2|^2 dx, \quad x \in \Omega, \tag{6}$$

where c_1 and c_2 are two constants which are the average intensities inside and outside the contour, respectively. With the level set method, we assume

$$\begin{cases} C = \{x \in \Omega : \phi(x) = 0\}, \\ \text{inside } (C) = \{x \in \Omega : \phi(x) > 0\}, \\ \text{outside } (C) = \{x \in \Omega : \phi(x) < 0\}. \end{cases}$$

By minimizing Eq. (6), we solve c_1 and c_2 as follows:

$$c_1(\phi) = \frac{\int_\Omega I(x) \cdot H(\phi)dx}{\int_\Omega H(\phi)dx}, \tag{7}$$

$$c_2(\phi) = \frac{\int_\Omega I(x) \cdot (1 - H(\phi))dx}{\int_\Omega (1 - H(\phi))dx}. \tag{8}$$

By incorporating the length and area energy terms into Eq. (6) and minimizing them, we obtain the corresponding variational level set formulation as follows:

$$\frac{\partial \phi}{\partial t} = \delta(\phi)\left[\mu\nabla\left(\frac{\nabla\phi}{|\nabla\phi|}\right) - v - \lambda_1(I - c_1)^2 + \lambda_2(I - c_2)^2\right], \tag{9}$$

where $\mu \geqslant 0$, $v \geqslant 0$, $\lambda_1 > 0$, $\lambda_2 > 0$ are fixed parameters, μ controls the smoothness of zero level set, v increases the propagation speed, and λ_1 and λ_2 control the image data driven force inside and outside the contour, respectively. ∇ is the gradient operator. $H(\phi)$ is the Heaviside function and $\delta(\phi)$ is the Dirac function. Generally, the regularized versions are selected as follows:

$$\begin{cases} H_\varepsilon(z) = \frac{1}{2}\left(1 + \frac{2}{\pi}\arctan\left(\frac{z}{\varepsilon}\right)\right), \\ \delta_\varepsilon(z) = \frac{1}{\pi} \cdot \frac{\varepsilon}{\varepsilon^2 + z^2}, \quad z \in R \end{cases}. \tag{10}$$

As shown in Fig. 1, if ε is too small, the values of $\delta_\varepsilon(z)$ tend to be near zero to make its effective range small, so the energy functional has a tendency to fall into a local minimum. The object may fail to be extracted if the initial contour starts far from it. In Section 4, we will give some examples to show this drawback. However, if ε is large, although $\delta_\varepsilon(z)$ tends to obtain a global minimum, the finial contour location may not be accurate [24].

3. The proposed model

3.1. The design of SPF function

The SPF function defined in [9] has values in the range $[-1, 1]$. It modulates the signs of the pressure forces inside and outside the region of interest so that the contour shrinks when outside the object, or expands when inside the object. Based on the analysis in Section 2, we construct the SPF function as follows:

$$spf(I(x)) = \frac{I(x) - \frac{c_1 + c_2}{2}}{\max\left(\left|I(x) - \frac{c_1 + c_2}{2}\right|\right)}, \quad x \in \Omega, \tag{11}$$

where c_1 and c_2 are defined in Eqs. (7) and (8), respectively.
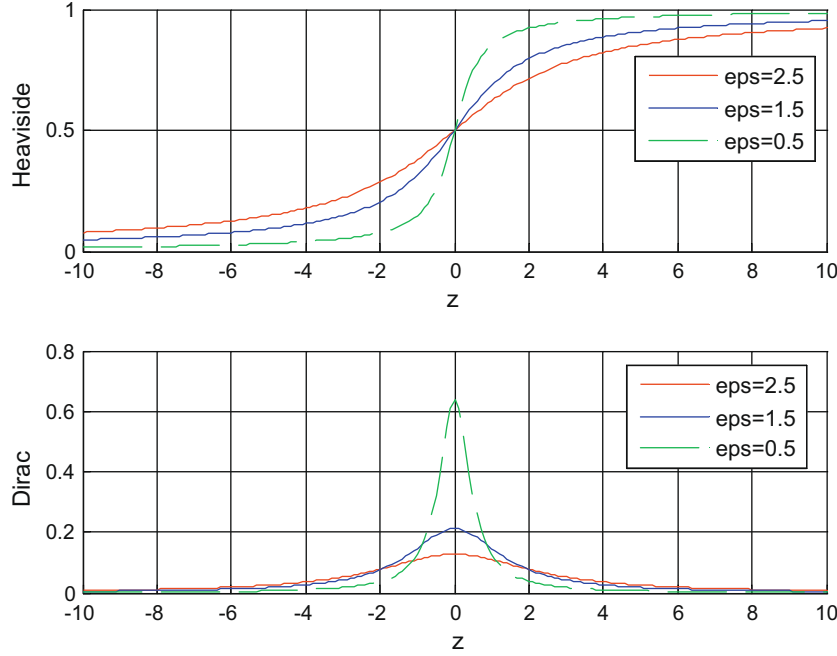
Fig. 1. The Heaviside function and Dirac function w.r.t different epsilon values.

The significance of Eq. (11) can be explained as follows. Refer to Fig. 2, we assume that the intensities inside and outside the object are homogeneous. It is intuitive that $\text{Min}(I(x)) \leqslant c_1$, $c_2 \leqslant \text{Max}(I(x))$, and the equal signs cannot be obtained simultaneously wherever the contour is. Hence, there is

$$\text{Min}(I(x)) < \frac{c_1 + c_2}{2} < \text{Max}(I(x)), \quad x \in \Omega. \tag{12}$$

Obviously, the signs of the SPF function in Eq. (11) are identical to what Fig. 2 shows, so Eq. (11) can serve as an SPF function. Substituting the SPF function in Eq. (11) for the ESF in Eq. (5), the level set formulation of the proposed model is as follows:

$$\frac{\partial \phi}{\partial t} = spf(I(x)) \cdot \left(\text{div}\left(\frac{\nabla\phi}{|\nabla\phi|}\right) + \alpha \right)|\nabla\phi| + \nabla spf(I(x)) \cdot \nabla\phi, \quad x \in \Omega \tag{13}$$

3.2. Implementation

In the traditional level set methods, the level set function is initialized to be an SDF to its interface in order to prevent it from being too steep or flat near its interface, and re-initialization is required in the evolution. Unfortunately, many existing re-initialization methods have an undesirable side effect of moving the zero level set away from its interface. Furthermore, it is difficult to decide when and how to apply the re-initialization. In addition, re-initialization is a very expensive operation. To solve these problems, we propose a novel level set method, which utilizes a Gauss-

ian filter to regularize the selective binary level set function after each iteration. The procedure of penalizing level set function to be binary is optional according to the desired property of evolution. If we want local segmentation property, the procedure is necessary; otherwise, it is unnecessary.

In our method, the level set function can be initialized to constants, which have different signs inside and outside the contour. This is very simple to implement in practice. In the traditional level set methods, the curvature-based term $\text{div}(\nabla\phi/|\nabla\phi|)|\nabla\phi|$ is usually used to regularize the level set function ϕ. Since ϕ is an SDF that satisfies $|\nabla\phi| = 1$ [13], the regularized term can be rewritten as $\Delta\phi$, which is the Laplacian of the level set function ϕ. As pointed out in [21] and based on the theory of scale-space [22], the evolution of a function with its Laplacian is equivalent to a Gaussian kernel filtering the initial condition of the function. Thus we can use a Gaussian filtering process to further regularize the level set function. The standard deviation of the Gaussian filter can control the regularization strength, just as the parameter μ in Eq. (9) does. Since we utilize a Gaussian filter to smooth the level set function to keep the interface regular, the regular term $\text{div}(\nabla\phi/|\nabla\phi|)|\nabla\phi|$ is unnecessary. In addition, the term $\nabla spf \cdot \nabla\phi$ in Eq. (13) can also be removed, because our model utilizes the statistical information of regions, which has a larger capture range and capacity of anti-edge leakage. Finally, the level set formulation of the proposed model can be written as follows:

$$\frac{\partial \phi}{\partial t} = spf(I(x)) \cdot \alpha|\nabla\phi|, \quad x \in \Omega. \tag{14}$$

The main procedures of the proposed algorithm are summarized as follows:

1. Initialize the level set function ϕ as

$$\phi(x, t=0) = \begin{cases} -\rho & x \in \Omega_0 - \partial\Omega_0, \\ 0 & x \in \partial\Omega_0, \\ \rho & x \in \Omega - \Omega_0, \end{cases} \tag{15}$$

where $\rho > 0$ is a constant, Ω_0 is a subset in the image domain Ω and $\partial\Omega_0$ is the boundary of Ω_0.
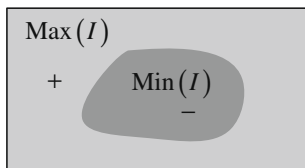

Fig. 2. The signs of the SPF function inside and outside the object are opposite.

2. Compute $c_1(\phi)$ and $c_2(\phi)$ using Eqs. (7) and (8), respectively.
3. Evolve the level set function according to Eq. (14).
4. Let $\phi = 1$ if $\phi > 0$; otherwise, $\phi = -1$.

This step has the local segmentation property. If we want to selectively segment the desired objects, this step is necessary; otherwise, it is unnecessary.

5. Regularize the level set function with a Gaussian filter, i.e. $\phi = \phi * G_\sigma$.
6. Check whether the evolution of the level set function has converged. If not, return to step 2.

Step 4 serves as a selective segmentation procedure, because it makes the deviation $|\nabla\phi|$ that is far from the interface of level set function ϕ close to zero, and only the $\phi(x)$ near the interface will evolve. Thus the evolution has local segmentation property. We can start the contour near the object of interest to obtain the desired segmentation. On the other hand, step 4 should be removed if we want to detect all the objects.
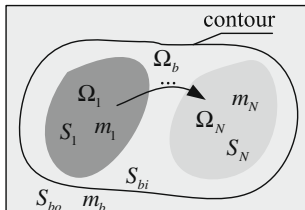
In step 5, the standard deviation σ of the Gaussian filter G_σ is a critical parameter, which should be chosen properly. If σ is too small, the proposed method will be sensitive to noise, and the evolution will be unstable. On the other hand, if σ is too large, edge leakage may occur, and the detected boundary may be inaccurate. In our experiments, we truncate the Gaussian kernel as a $K \times K$ mask for efficiency, which K is typically less than 6. σ ranges from 0.8 to 1.5.

3.3. Discussion for segmenting multi-objects with different intensities

Since our model utilizes the global image intensities inside and outside the contour, it has the similar drawbacks to the C–V model, such as the inefficiency in handling images with severe intensity inhomogeneity. However, if the intensities of objects in the images are homogeneous in their own domains while being different from each other, our model can still handle some of these cases well.

As shown in Fig. 3, we assume that there are N objects in the image, and then the image domain is partitioned into $\Omega_1, \ldots, \Omega_N$ and Ω_b, whose intensities are $m_1, \ldots, m_N$ and m_b, respectively. The object areas are denoted as $S_1, \ldots, S_N$. The contour is set around the objects. The background areas inside and outside the contour are S_{bi} and S_{bo}, respectively. As Fig. 3 shows, we only consider the case that the background intensity is the highest. The discussion is also suitable for the case when the background intensity is the lowest. However, similar to the C–V model [15,24], our model cannot handle the case when the background intensity is neither the highest nor the lowest. For the convenience of discussion, we assume $m_1 \leqslant m_2 \leqslant \ldots m_N \leqslant m_b$.

Parameters c_1 and c_2 serve as the average intensities which can be written as

$$\begin{cases} c_1 = \left(\sum_{k=1}^{N} m_k S_k + m_b S_{bi}\right) \Big/ \left(\sum_{k=1}^{N} S_k + S_{bi}\right), \\ c_2 = m_b, \end{cases} \quad (16)$$

So the SPF function is as follows:

$$spf(I(x)) = I(x) - \frac{\left(\sum_{k=1}^{N} m_k S_k + m_b S_{bi}\right) \Big/ \left(\sum_{k=1}^{N} S_k + S_{bi}\right) + m_b}{2}, \quad x \in \Omega. \quad (17)$$

Eq. (17) can be rewritten as

$$spf(I(x)) = \frac{(I(x) - m_b)S_{bi} + \sum_{k=1}^{N}\left(I(x) - \frac{m_b + m_k}{2}\right)S_k}{\sum_{k=1}^{N} S_k + S_{bi}}, \quad x \in \Omega, \quad (18)$$

Thus

$$spf(I(x)) = \sum_{k=1}^{N}\left(\frac{m_b - m_k}{2}\right)S_k \Big/ \left(\sum_{k=1}^{N} S_k + S_{bi}\right) > 0, \quad \text{for } x \in \Omega_b$$
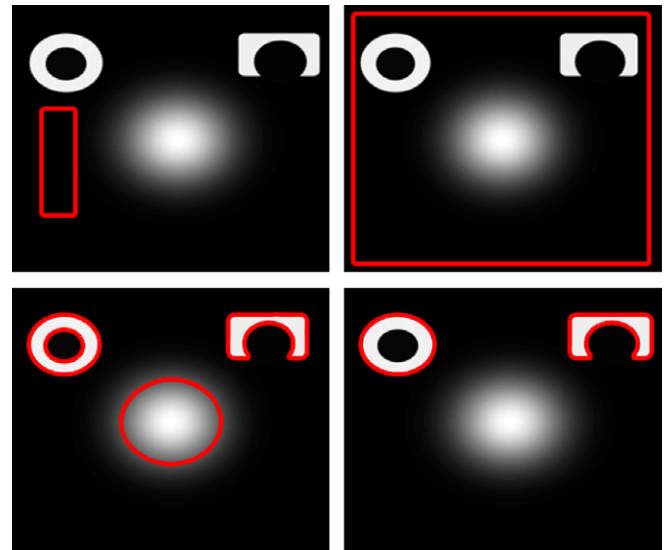
When $x \in \Omega_N$, there is

$$spf(I(x)) = \frac{(m_N - m_b)S_{bi} + \sum_{k=1}^{N}(m_N - \frac{m_b + m_k}{2})S_k}{\sum_{k=1}^{N} S_k + S_{bi}}. \quad (19)$$

If $m_N \leqslant (m_b + m_1)/2$, then $spf(I(x)) < 0$ for all $x \in \Omega_1, \ldots, \Omega_N$, and our model can handle these images well; otherwise, our model may fail. It is worth noting that the C–V model may also fail in this case because its energy functional can be easily trapped into local minima [5].

### 3.4. Advantages of our model over the GAC and C–V models

In contrast to the GAC model, our model utilizes the image statistical information to stop the curve evolution on the desired boundaries, so it is robust to noise. Furthermore, our model can well handle images with weak edges or without edges. In addition, our model can extract the interior boundaries of the objects by setting the initial contour anywhere.

Compared with the C–V model, our model can extract objects whose boundaries are distinctive while interior intensities are not homogeneous (see Fig. 7 in Section 4 for example). Moreover,

Fig. 3. Demonstration of segmentation for multi-objects with different intensities. $m_1, \ldots, m_N$ are object intensities, respectively, and $S_1, \ldots, S_N$ are object areas. S_{bi} and S_{bo} are background areas inside and outside objects. m_b is background intensity. $\Omega_1, \ldots, \Omega_N$ are object domains, and Ω_b is background domain.

Fig. 4. The segmentation results on a synthetic image by the proposed method and the GAC model. The first row shows the initial contours of our method (left) and the GAC model (right), respectively, and the second row shows the corresponding segmentation results. The parameter $\alpha = 20$.
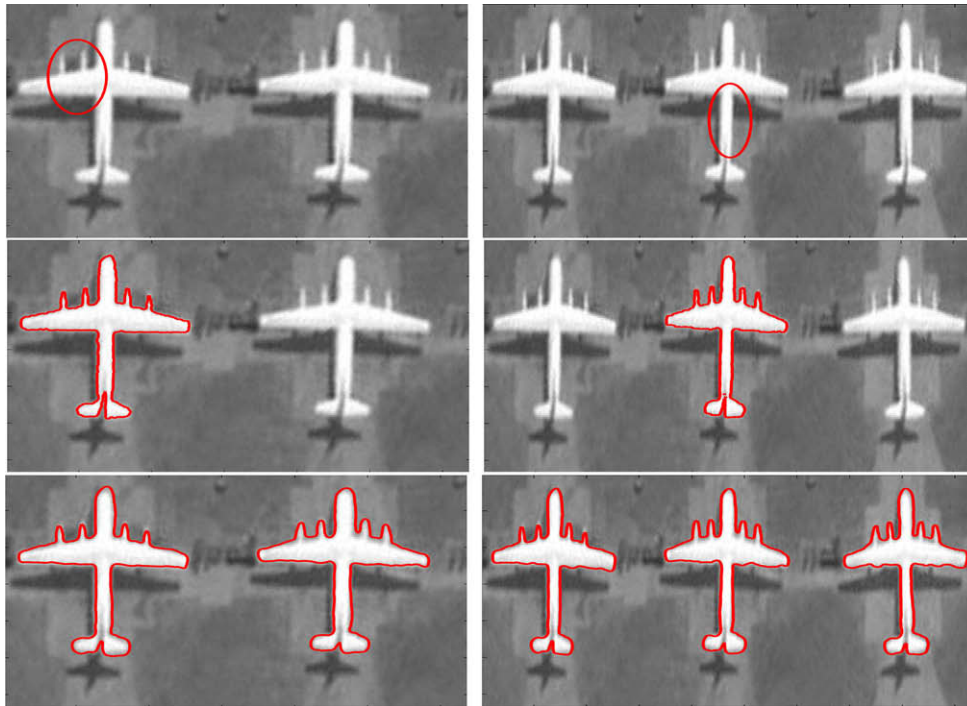
Fig. 5. Comparisons of the global segmentation property between the C–V model and the proposed method. The first row shows the initial contours, the second row shows the segmentation results of C–V model, and the third row shows the segmentation results of the proposed method. The parameter $\alpha = 20$.

our model can selectively extract the desired object by setting the initial contour intersecting or surrounding the desired boundaries, while the C–V model will extract all the objects. Furthermore, the evolution direction in our model can be controlled to obtain satisfying segmentation results, while the C–V model may get disordered results (see Fig. 8 in Section 4 for example). In addition, our model can extract all the objects with the initial contour being set anywhere, while the C–V model may be trapped into the local minima and then result in unsatisfied segmentation (see Fig. 5 in Section 4 for example). Finally, our model has less computational complexity than the GAC and C–V models.

4. Experimental results

Our algorithm is implemented in Matlab 7.0 on a 2.8-GHz Intel Pentium IV PC. In each experiment, we choose $\rho = 1$, $\varepsilon = 1.5$, $\sigma = 1$, $K = 5$, and time step $\Delta t = 1$. The values of α were set according to the images. The Matlab source code of the proposed algorithm can be downloaded at http://www.comp.polyu.edu.hk/~cslzhang/code/IVC.zip.

Fig. 4 shows the segmentation results of a synthetic image with objects having weak edges and interior holes. The GAC model with the traditional level set method is used in the comparison. The size of the test image is 250×250 pixels. The left column in the first row of Fig. 4 shows the initial contour of our model, which is not around or inside the objects, while all of the objects are surrounded by the initial contour of the GAC model (see the right column in the first row of Fig. 4). The second row shows the corresponding segmentation results of our method and the GAC model, respectively. For our method, the evolution of the level set function converges in 30 iterations and takes only 0.25 min, while for the traditional GAC model, the evolution converges in 7000 iterations and takes for 45 min. Our method accurately detects the exterior and interior boundaries of the objects, as well as the weak edge object, whereas the traditional GAC model fails to detect the interior boundary of the object and the weak edge object.

Fig. 5 demonstrates the global segmentation property of our method. The initial contour is far from the objects, as shown in the first row of Fig. 5. The second row shows the segmentation results of the C–V model, which fails to extract all the objects, whereas our method could accurately extract all the objects, as shown in the third row of Fig. 5.

Fig. 6 shows the segmentation results of two galaxy images by the proposed method. The first row shows the initial contours which are around the objects. The second row shows the segmentation results. We see that the contours of the galaxies are accurately detected.

Fig. 7 demonstrates the selective segmentation property of the proposed method. The size of the test image is 60×80 pixels.
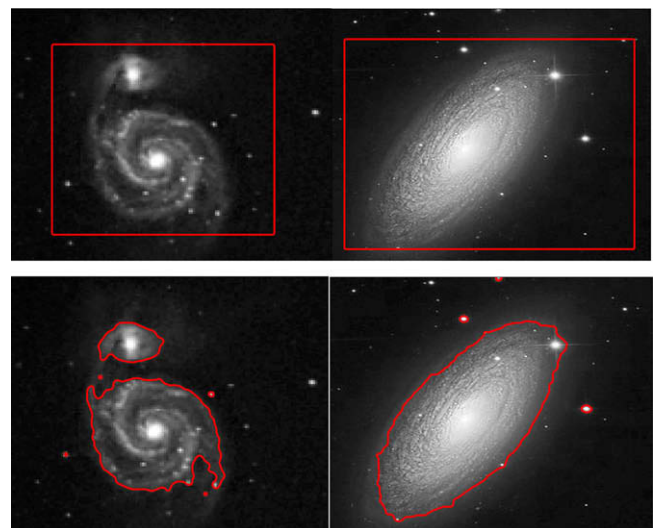
Fig. 6. Segmentation results of the galaxy images. The first row shows the initial contours and the second row show the segmentation results. The parameter $\alpha = 20$.
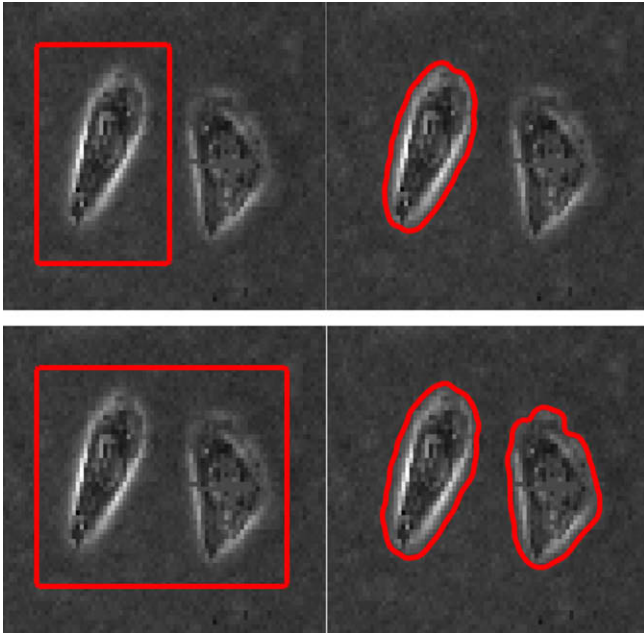
Fig. 7. Selective segmentation results for a real microscope cell image. The left column shows the initial contours, and the right column shows the corresponding segmentation results. The parameter $\alpha = 20$.

The evolution of the level set function converges in 20 iterations within 0.1 min. As we can see from the experiment, by setting the initial contours close to the desired object (left column in Fig. 7), the desired segmentation results can be obtained (the right column in Fig. 7).

Fig. 8 demonstrates the proposed method in medical image segmentation. The left two columns of Fig. 8 show two magnetic resonance images of the left ventricle of a human heart, and the right two columns show two noisy ultrasound images of the same organ. The third row shows the corresponding segmentation results of the proposed method, which are obviously more accurate than the corresponding segmentation results of the C–V model that are shown in the second row.

Fig. 9 compares the proposed method and the GAC model by applying them to an MR image of corpus callosum. The size of the test image is 116×62 pixels. Fig. 9a shows the initial contour. For the proposed method (see Fig. 9b), the evolution of the level set function converges in 150 iterations and takes only 0.2 min, while for the traditional GAC model with a small balloon force $\alpha = 0.6$, the evolution converges in 7000 iterations and takes 35 min, and the contour could not pass through the narrow and long part of the object (see Fig. 9c). With a larger balloon force $\alpha = 0.8$, the contour could pass over the relatively weaker part of the object (see Fig. 9d), and the evolution converges in 6000 iterations and takes 30 min.

Fig. 10 shows our method in processing some more general datasets of MR image of corpus callosum. The first and third rows show the initial contours, which are far away from the thin parts of the objects. The second and fourth rows show the segmentation results. We only need to tune the parameter α to get the desired results. As we can see from Fig. 10, although some corpus callosums are very narrow in regions, and some have a very large gap between the corpus callosum and fornix, our method can still achieve satisfying segmentation results by setting a proper value of α.

We use Fig. 11 to illustrate our conclusion in Section 3.3. The number of objects is $N = 3$. In Fig. 11c, $m_1 = 50$, $m_2 = 100$, $m_3 = 120$, $m_b = 200$, $m_3 < (m_b + m_1)/2$, and the segmentation result
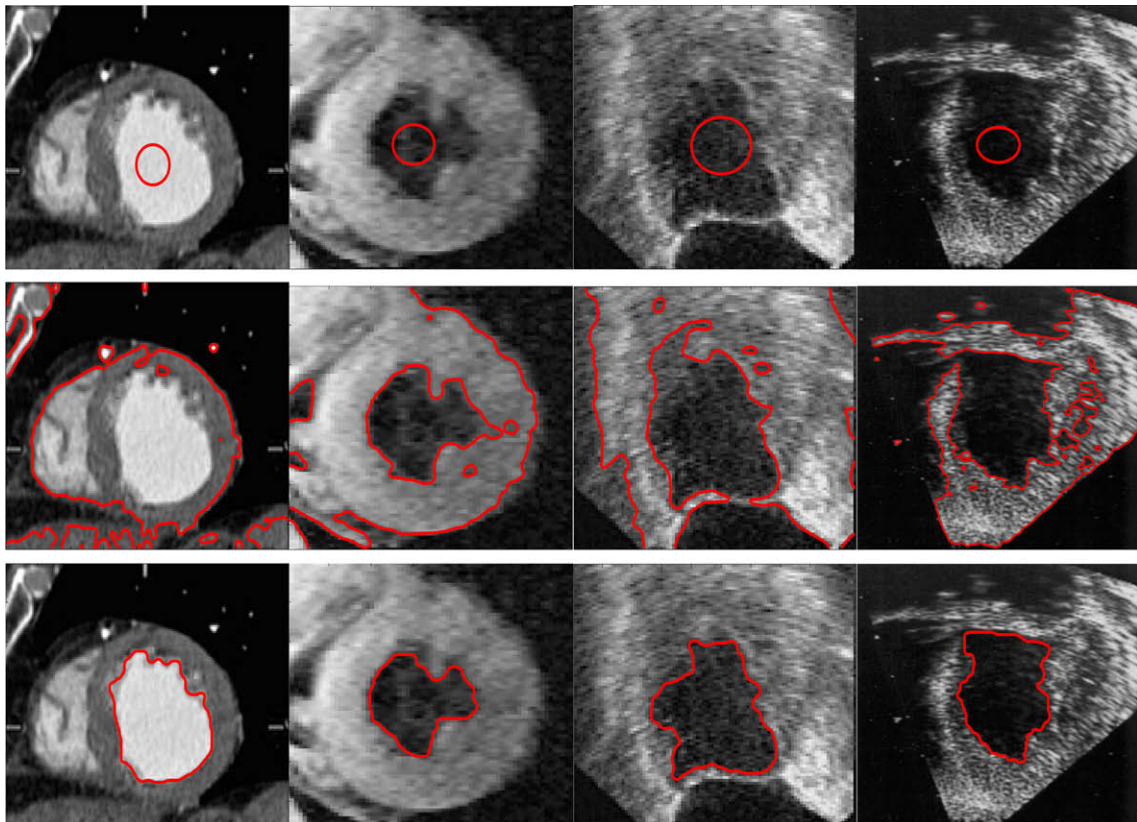
Fig. 8. First row shows the initial contours. The segmentation results by the C–V model are shown in the second row, and the segmentation results by our model are in the third row. We choose $\alpha = 5$ for the left three columns, and $\alpha = 10$ for the most right column.
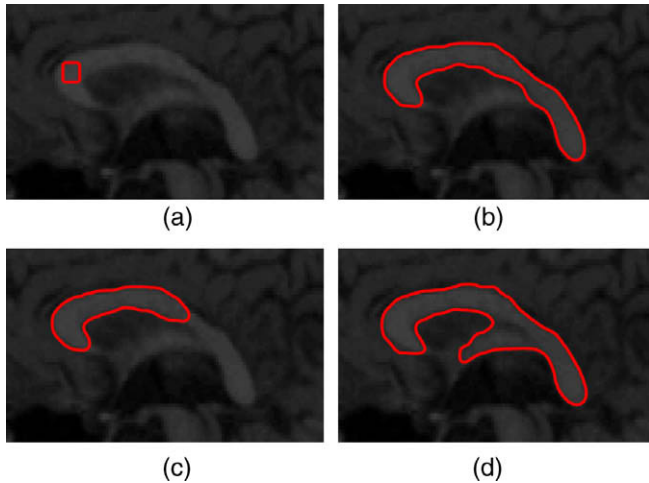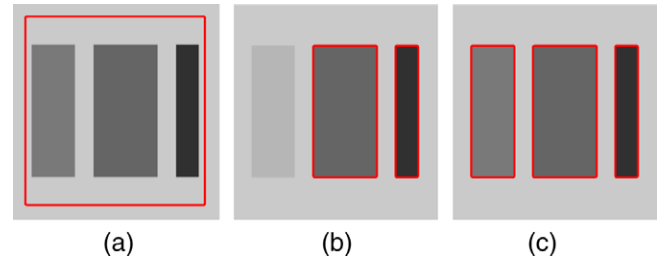
Fig. 9. (a) Initial contour. (b) Segmentation result of our model, $\alpha = 5$. (c) Segmentation result of the GAC model by setting $\alpha = 0.6$. (d) Segmentation result of the GAC model by setting $\alpha = 0.8$.


Fig. 11. Results for segmenting multi-objects with three different intensities. (a) Initial contour. (b) Segmentation result by setting $\alpha = 10$. The background intensity is 200, and the intensities of objects from left to right are 180, 100, and 50, respectively. (c) Segmentation result by setting $\alpha = 10$. The background intensity is 200, and the intensities of objects from left to right are 120, 100, and 50, respectively. The C–V model has similar segmentation results.

is satisfactory. In Fig. 11b, $m_1 = 50$, $m_2 = 100$, $m_3 = 180$, $m_b = 200$, $m_3 > (m_b + m_1)/2$, one object failed to extract. The C–V model has similar segmentation results on this example.

The last experiment tests the effect of parameter α on the segmentation results. After the segmentation converges, we compute the pixels deviated from the areas inside and outside the true boundary, which is called the Area Error Measure (AEM) [23]. We tested our method on an object with a long, narrow protrusion as shown in Fig. 12. The image was added with Gaussian noise with standard deviation 0.05. As shown in Fig. 12a, if we choose a small value of σ, the regularized capacity of Gaussian smoothing in our

method will be weak, and hence the value of AEM will be large and the segmentation results will be very noisy (refer to the second columns in Fig. 12b and c). With the increasing of σ, the value of AEM decreases, and the segmentation results get satisfying. The segmentation results when AEM reaches the minimum are shown in the third columns of Fig. 12b and c. However, if the value of α is not large enough while the value of σ is too large, the surface of level set function will be over-smoothed and then the contour will not be able to flow into the narrow region of the object (see the most left image in Fig. 12b), and the value of AEM will increase (see the curves in Fig. 12a). This problem can be solved by choosing a larger α because a larger α will increase the shrinking or expanding capacity of curve evolution to make the contour be able to flow into narrow regions. Refer to the blue curve in Fig. 12a, when we set $\alpha = 10$, we can get small AEM values in a large range of σ, and the corresponding segmentation result is shown in the most right column of Fig. 12c.
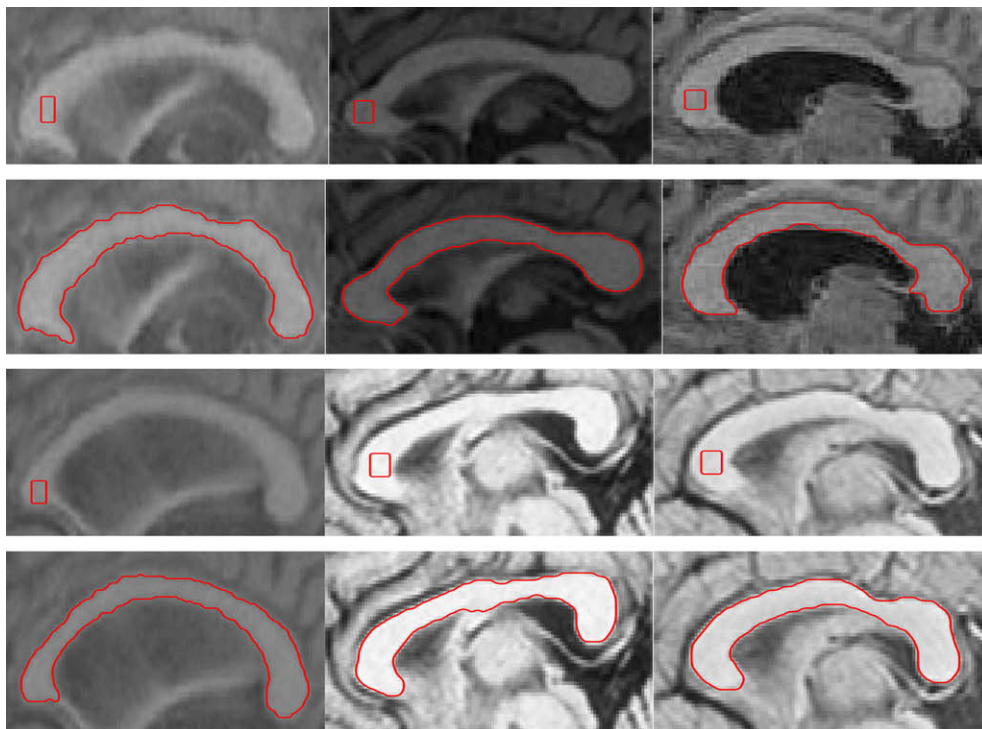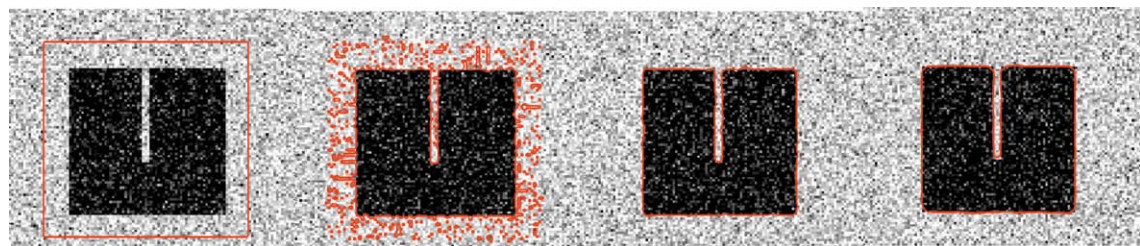

Fig. 10. The images in the first and third rows show the initial contours. The second and fourth rows show the corresponding segmentation results. We set $\alpha = 6.3$ for the most left image in the second row and the most right image in the fourth row, and $\alpha = 5$ for other images.
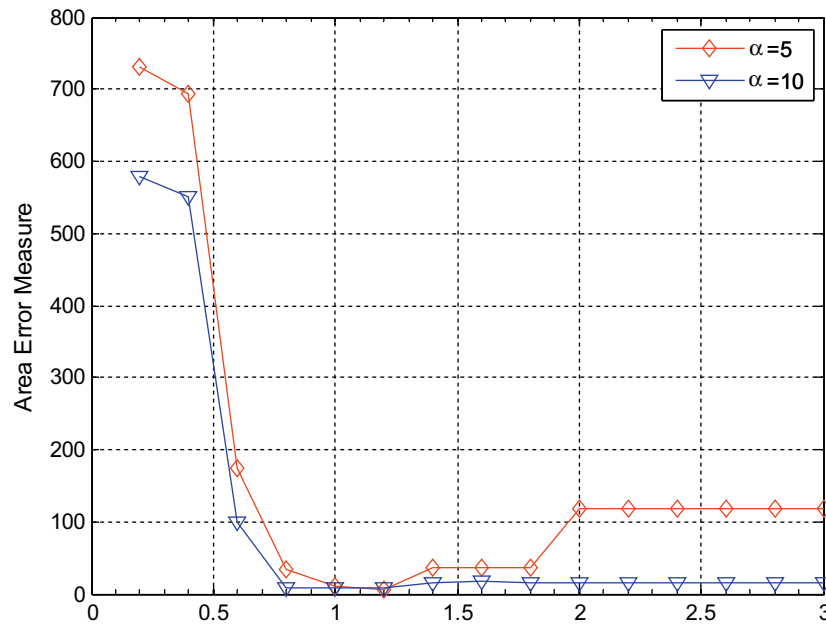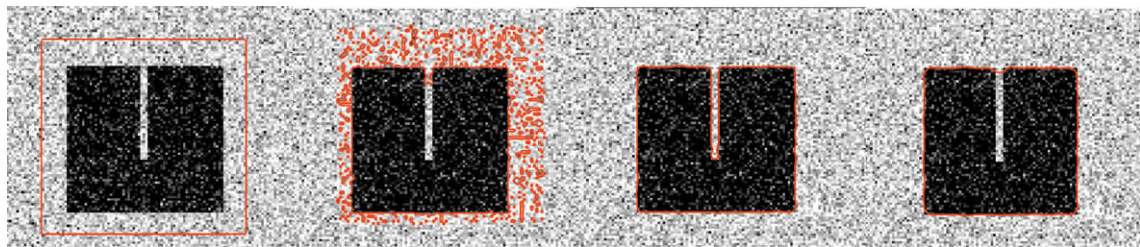
Fig. 12. (a) The Area Error Measure curves w.r.t the standard deviation σ of the Gaussian filter. (b) The initial contour (left) and the experimental results (right) by setting $\sigma = 0.2$, 1 and 2.5 with $\alpha = 5$. (c) The initial contour (left) and the experimental results (right) by setting $\sigma = 0.2$, 1 and 2.5 with $\alpha = 10$.

5. Conclusion

In this paper, we proposed a novel region-based ACM for image segmentation which is implemented with a new level set method named SBGFRLS method. The SBGFRLS method reduces the expensive re-initialization of the traditional level set method to make it more efficient. The proposed model implementing with the SBGFRLS method combines the merits of the traditional GAC and C–V models, which possesses the property of local or global segmentation. Extensive experiments on synthetic and real images demonstrated the advantages of the proposed method over the classical ACMs with the traditional level set methods, such as the GAC and C–V models. Our proposed SBGFRLS method is general and robust which can be applied to implementing the algorithms of some classical ACMs, such as GAC model [3,4], C–V model [5], PS model [14,15], LBF model [11,24], and so on.

References

[1] M. Kass, A. Witkin, D. Terzopoulos, Snakes: active contour models, International Journal of Computer Vision 1 (1988) 321–331.
[2] N. Xu, N. Ahuia, R. Bansal, Object segmentation using graph cuts based active contours, Computer Vision and Image Understanding 107 (2007) 210–224.

[3] V. Caselles, R. Kimmel, G. Sapiro, Geodesic active contours, in: Processing of IEEE International Conference on Computer Vision'95, Boston, MA, 1995, pp. 694–699.

[4] V. Caselles, R. Kimmel, G. Sapiro, Geodesic active contours, International Journal of Computer Vision 22 (1) (1997) 61–79.

[5] T. Chan, L. Vese, Active contours without edges, IEEE Transaction on Image Processing 10 (2) (2001) 266–277.

[6] G.P. Zhu, Sh.Q. Zhang, Q.SH. Zeng, Ch.H. Wang, Boundary-based image segmentation using binary level set method, Optical Engineering 46 (2007) 050501.

[7] J. Lie, M. Lysaker, X.C. Tai, A binary level set model and some application to Munford–Shah image segmentation, IEEE Transaction on Image Processing 15 (2006) 1171–1181.

[8] D. Mumford, J. Shah, Optimal approximation by piecewise smooth function and associated variational problems, Communication on Pure and Applied Mathematics 42 (1989) 577–685.

[9] C.Y. Xu, A. Yezzi Jr., J.L. Prince, On the relationship between parametric and geometric active contours, in: Processing of 34th Asilomar Conference on Signals Systems and Computers, 2000, pp. 483–489.

[10] C.M. Li, C.Y. Xu, C.F. Gui, M.D. Fox, Level set evolution without re-initialization: a new variational formulation, in: IEEE Conference on Computer Vision and Pattern Recognition, San Diego, 2005, pp. 430–436.

[11] C.M. Li, C. Kao, J. Gore, Z. Ding, Implicit active contours driven by local binary fitting energy, in: IEEE Conference on Computer Vision and Pattern Recognition, 2007.

[12] N. Paragios, R. Deriche, Geodesic active contours and level sets for detection and tracking of moving objects, IEEE Transaction on Pattern Analysis and Machine Intelligence 22 (2000) 1–15.

[13] S. Osher, R. Fedkiw, Level Set Methods and Dynamic Implicit Surfaces, Springer-Verlag, New York, 2002.

[14] A. Tsai, A. Yezzi, A.S. Willsky, Curve evolution implementation of the Mumford–Shah functional for image segmentation, denoising, interpolation, and magnification, IEEE Transaction on Image Processing 10 (2001) 1169–1186.

[15] L.A. Vese, T.F. Chan, A multiphase level set framework for image segmentation using the Mumford–Shah model, International Journal of Computer Vision 50 (2002) 271–293.

[16] R. Ronfard, Region-based strategies for active contour models, International Journal of Computer Vision 46 (2002) 223–247.

[17] N. Paragios, R. Deriche, Geodesic active regions and level set methods for supervised texture segmentation, International Journal of Computer Vision 46 (2002) 223–247.

[18] C. Xu, J.L. Prince, Snakes, shapes, and gradient vector flow, IEEE Transaction on Image Processing 7 (1998) 359–369.

[19] G. Aubert, P. Kornprobst, Mathematical Problems in Image Processing: Partial Differential Equations and the Calculus of Variations, Springer, New York, 2002.

[20] A. Vasilevskiy, K. Siddiqi, Flux-maximizing geometric flows, IEEE Transaction on Pattern Analysis and Machine Intelligence 24 (2002) 1565–1578.

[21] Y. Shi, W.C. Karl, Real-time tracking using level sets, IEEE Conference on Computer Vision and Pattern Recognition 2 (2005) 34–41.

[22] P. Perona, J. Malik, Scale-space and edge detection using anisotropic diffusion, IEEE Transaction on Pattern Analysis and Machine Intelligence 12 (1990) 629–640.

[23] C. Davatzikos, J.L. Prince, An active contour model for mapping the cortex, IEEE Transaction on Medical Imaging 14 (1995) 65–80.

[24] C. Li, C. Kao, J.C. Gore, Z. Ding, Minimization of region-scalable fitting energy for image segmentation, IEEE Transaction on Image Processing 17 (2008) 1940–1949.